ELSEVIER

Contents lists available at ScienceDirect

Computers in Biology and Medicine

journal homepage: www.elsevier.com/locate/compbiomed





Unsupervised separation of nonlinearly mixed event-related potentials using manifold clustering and non-negative matrix factorization

Kai Zhang ^a, Xiaogang Hu ^{a,b,c,d,e,*}

- ^a Department of Mechanical Engineering, Pennsylvania State University, University Park, USA
- ^b Department of Kinesiology, Pennsylvania State University, University Park, USA
- ^c Department of Physical Medicine & Rehabilitation, Pennsylvania State Hershey College of Medicine, USA
- ^d Huck Institutes of the Life Sciences, Pennsylvania State University, University Park, USA
- e Center for Neural Engineering, Pennsylvania State University, University Park, USA

ARTICLE INFO

Keywords: Electroencephalogram Event related potential Non-linear source mixture Manifold clustering Non-negative matrix factorization

ABSTRACT

Event-related potentials (ERPs) can quantify brain responses to reveal the neural mechanisms of sensory perception. However, ERPs often reflect nonlinear mixture responses to multiple sources of sensory stimuli, and an accurate separation of the response to each stimulus remains a challenge. This study aimed to separate the ERP into nonlinearly mixed source components specific to individual stimuli. We developed an unsupervised learning method based on clustering of manifold structures of mixture signals combined with channel optimization for signal source reconstruction using non-negative matrix factorization (NMF). Specifically, we first implemented manifold learning based on Local Tangent Space Alignment (LTSA) to extract the spatial manifold structure of multi-resolution sub-signals separated via wavelet packet transform. We then used fuzzy entropy to extract the dynamical process of the manifold structures and performed a k-means clustering to separate different sources. Lastly, we used NMF to obtain the optimal contributions of multiple channels to ensure accurate source reconstructions. We evaluated our developed approach using a simulated ERP dataset with known ground truth of two components of ERP mixture signals. Our results show that the correlation coefficient between the reconstructed source signal and the true source signal was 92.8 % and that the separation accuracy in ERP amplitude was 91.6 %. The results show that our unsupervised separation approach can accurately separate ERP signals from nonlinear mixture source components. The outcomes provide a promising way to isolate brain responses to multiple stimulus sources during multisensory perception.

1. Introduction

Understanding brain responses through electroencephalograms (EEG), magnetic resonance imaging (MRI), and functional magnetic resonance imaging (fMRI) has proven to be an effective approach for understanding neural mechanisms during brain processing of external stimuli [1–4]. EEG, in particular, is extensively utilized due to its high temporal resolution, non-invasive nature, and cost efficiency [5]. Event-related potentials (ERP) of EEG, a commonly used paradigm in sensory response, provide insights into the brain's response to external sensory stimuli and facilitate the investigation of fundamental principles of multisensory integration [6–8]. Sensory processing by the brain typically results from the integration of multiple sources of sensory stimuli. Isolating individual responses to individual stimuli requires

effective separation from mixture ERPs and a comprehensive understanding of the interaction between different sensory perception sources. Perceptual integration strategies in various models can be broadly classified into two categories: neural responses to multisensory stimulation are mixed without interaction [9], and neural responses are not only nonlinearly mixed but also interactive. The interaction in audiovisual perception exemplifies the first model [10], while tactile perception (from afferent fibers below the skin and sensory receptors in the skin) induced by transcutaneous electrical stimulation is representative of the latter [11]. However, understanding the interactive principles and signal representation in these models remains a challenge, particularly in distinguishing sources in nonlinearly interactive mixture ERPs. These challenges include the poor spatial resolution due to the volume conduction effect, where brain response signals become diffused

https://doi.org/10.1016/j.compbiomed.2024.108700

Received 29 January 2024; Received in revised form 12 May 2024; Accepted 1 June 2024 Available online 4 June 2024

0010-4825/© 2024 Elsevier Ltd. All rights are reserved, including those for text and data mining, AI training, and similar technologies.

^{*} Corresponding author. Department of Mechanical Engineering, Pennsylvania State University, University Park, USA. *E-mail address:* xxh120@psu.edu (X. Hu).

and attenuated as they travel through head tissues to the scalp surface. This leads to substantial signal overlap at scalp electrodes from different brain regions, complicating the localization of source information [12]. In addition, unlike the separation of mixed stimuli in additive models, certain stimuli (e.g., multisensory perception evoked by transcutaneous electrical stimulation) exhibit complex interactions among sources without ground truth of individual responses.

Over the past few years, various strategies have been developed for mixture signal separation. For instance, Independent Component Analysis (ICA), a common technique for blind source separation, employs a linear transformation to decompose mixed signals into statistically independent source signals [13]. In addition, time contrastive learning and spatial filters [14–18] use matrix transformation or temporal feature segmentation to separate source signals. However, these strategies may not be suitable for non-linear mixing and source-interactive signals. Wavelet transform, on the other hand, can decompose raw EEGs into multi-resolution time and frequency representations, offering insights into both local structures and global waveforms [19]. By extracting potential features of source and channel correlations at different scales, and employing clustering techniques to classify sub-signals, one can effectively reconstruct source signals corresponding to individual brain responses.

Recent studies have also explored various strategies for nonlinear feature extraction [20]. Manifold learning, for instance, has proven to be effective to uncover low-dimensional structures and intrinsic signal features, better than traditional linear methods in identifying and separating different patterns [21,22]. It can preserve local data proximity and accurately reconstruct the inherent structure of source signals [23]. Although manifold structures can reflect the spatial structure of signals, they lack the capacity to describe the dynamic evolution of these structures. Entropy, as a measure of dynamic properties, can reveal the complexity and dynamic evolution of signals [24]. It has been shown to be effective in evaluating dynamic processes in manifold structures [25], extracting distinct information of various trajectories. By integrating the strengths of manifold learning and entropy analysis, one could extract nonlinear dynamic features of signals, providing a foundation for source separation.

In source signal reconstruction, the interaction between channels can be significant. Multichannel signals often contain redundant and irrelevant components, and channel optimization can enhance the extraction of original signals or specific stimulus-related feature components [26]. The representation of mixture signals can arise from the superposition of different subcomponents and from the varying contributions of different channels. Hence, channel optimization presents a promising approach to enhancing the separation and reconstruction of source signals.

To separate nonlinearly mixed and interactive signals from mixture ERPs, this study developed a strategy based on manifold learning cluster and non-negative matrix factorization (NMF) for ERP source separation from a mixture signal (Fig. 1). Specifically, we employed manifold learning based on Local Tangent Space Alignment (LTSA), which delineates the spatial manifold configuration of multi-resolution sub-signals derived after wavelet packet decomposition. Subsequently, the dynamic features of the manifold structure were extracted using fuzzy entropy, followed by the application of unsupervised k-means clustering for the separation of different sources. Additionally, we adopted NMF to optimize the contribution from different EEG channels during source reconstruction to consider the different impact of multiple channels.

The research framework is visualized in Fig. 1. The main contribution of this study was the development of a novel unsupervised method to separate the source ERP of different stimuli from mixture ERP, especially for nonlinear mixture responses. To accurately decompose the ERP source signals, we employed nonlinear manifold learning and fuzzy entropy to extract the inherent dynamic features of each source component. The simulation results demonstrated that our method could effectively reconstruct source signals in terms of ERP amplitude, latency, and waveform. The outcomes provide a new approach that can help to understand neural mechanisms of multi-sensory perceptions.

2. Methodology

In this section, we first describe the data acquisition steps. We then describe the individual steps of the source separation algorithm. Lastly, we describe the evaluation processes, including the comparison with existing methods and an ablation study that evaluated the benefits of

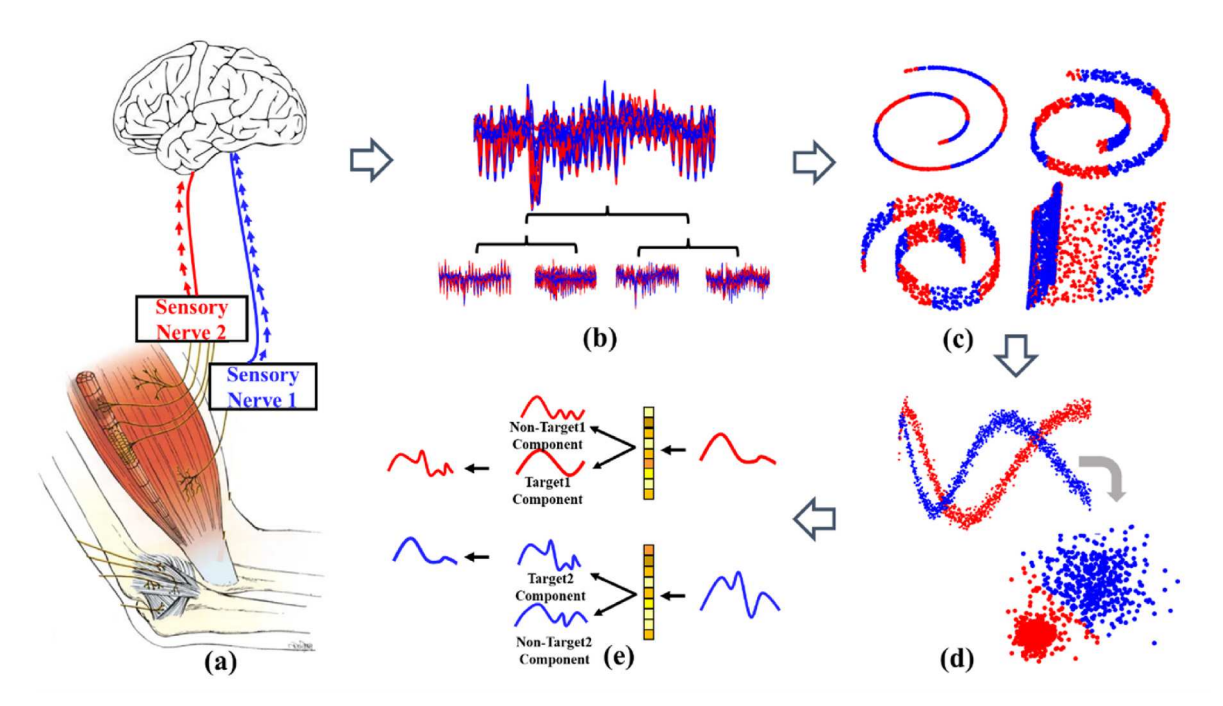


Fig. 1. Diagram of separation strategy. (a) Example of multisensory perception model. (b) EEG decomposition based on wavelet packet transform. (c) Using manifold learning to obtain spatial manifold structure of sub-signals. (d) Performing fuzzy entropy to extract dynamic process of manifold structure and cluster separation. (e) Applying NMF to obtain the optimal contributions of multiple channels.

different processing steps.

2.1. Dataset simulation

Due to the lack of prior knowledge or ground-truth representation of individual responses, it is difficult to validate our separation algorithms without labeled information. To assess the performance of our separation strategy, we collected real EEG data from four healthy human subjects (age range: 23–36 years) who participated in a tactile stimulation experiment evoked by transcutaneous electrical stimulation. The stimulation protocol details are provided in previous studies [27] and are summarized in the Supplementary Material. They gave informed consent with protocols approved by the Institutional Review Board of Penn State University.

EEG data were acquired using a BrainAmp DC amplifier, with a frequency range of 0.015–250 Hz and a sampling rate of 1000 Hz. Data from 32 electrodes, including a reference electrode at the right mastoid, were collected. The data were with a band-pass filter set at 0.1–100 Hz and a 50 Hz notch filter. Additionally, a Butterworth band-pass filter was applied to restrict the frequency range to 0.1–30 Hz, to eliminate electrical stimulus artifacts and irrelevant noise. Independent Component Analysis (ICA) was employed to remove artifacts related to blinking, horizontal, and vertical eye movements.

Given the considerable variability in EEG representations across individuals, we treated the EEG data from each subject as a separate source and generated six mixed datasets. This approach retained the EEG feature inherent to each subject while simulating the complex interactions in real EEG data. The data mixing procedure was calculated by:

$$S_{M} = \alpha \cdot \sigma(s_{1}) + (1 - \alpha) \cdot \sigma(s_{2})$$

$$\sigma(s_{label}) = \frac{1}{1 + e^{-s_{label}}}$$

Where s_{label} (label = 1, 2) represents the source signal with a dimension of $m \times t$, m, t represents the numbers of channels and sample data points, s_M is the mixture signal and α is the weight of the mixture. To simulate

the interactive relation between different sources during mixture, we calculated α as:

$$\overline{s_1} = \frac{1}{mt} \sum_{m=1}^{m} \sum_{t=1}^{t} s_{1mt}, \overline{s_2} = \frac{1}{mt} \sum_{m=1}^{m} \sum_{t=1}^{t} s_{2mt}$$

$$\alpha = \frac{|\overline{s_1}|}{|\overline{s_1} + \overline{s_2}|}$$

Where $\overline{s_1}$ and $\overline{s_2}$ are mean values of signal sources. The above mixing process not only satisfies the nonlinear mixing relation, but also meets the requirement of interactive sources. The simulation strategy is shown as Fig. 2:

Fig. 2 illustrates that the mixed EEG signals closely mirror the waveform feature of the source ERPs, maintaining the integrity of the original signal features. Notably, these signals preserved a significant N300 peak and reliable latency features, indicating that the mixed signals meet essential criteria for our algorithm testing and evaluation.

2.2. Signal decomposition using wavelet packet transform

Continuous EEG could be decomposed into a convolution of a series of basic functions (i.e. wavelets) with specific time and frequency properties, which are widely used to obtain multi-resolution sub-signals of EEG [28,29]. In our work, we obtained EEG signals with a mixed signal matrix of 28 (channels) × 3000 (sample points), after removing the ocular and reference electrodes. Then, the simulated mixed EEG signals were decomposed into a set of wavelet packet nodes in the form of a full binary tree by wavelet packet transform (WPT). Empirical Mode Decomposition (EMD) is a commonly used method for the decomposition of bio-signals. EMG can decompose signals into a finite number of Intrinsic Mode Functions (IMFs). Different IMF components represent different oscillation scales of the signal, but the IMFs cannot be used to represent the original signal waveforms of different sources, with each source containing a range of frequency content. EMD does not rely on any basis functions and can adaptively generate intrinsic modal functions based on the analyzed signal. In contrast, the WPT employed in our study involves the selection and optimization of basis function

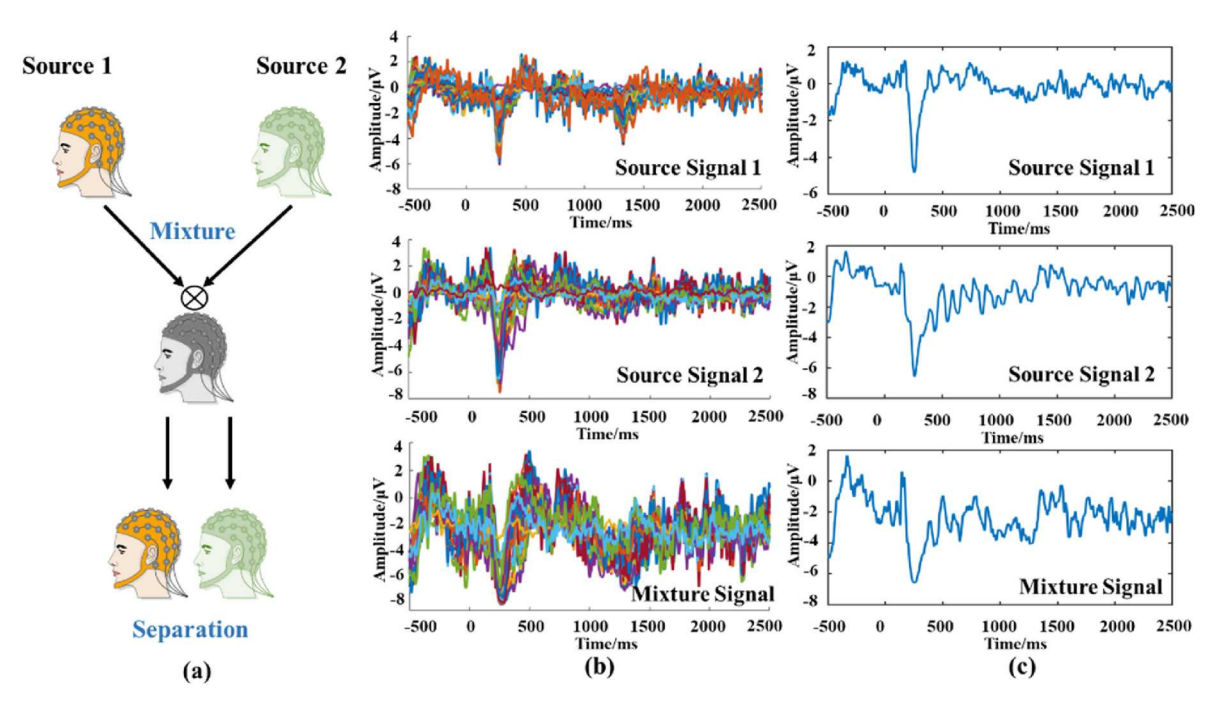


Fig. 2. EEG signal simulation strategy. (a). Apply ERP from individual subjects to simulate the brain responses for individual stimuli. Using a nonlinear function to mix different sources. The signal mixture was then separated using our algorithm. (b). Representation of simulation ERP signals of all 32 channels. Different colors indicate ERPs from different channels. (c). Representation of simulation ERP signals of a single representative channel.

parameters. The decomposed components contain multiple frequency bands with high frequency resolutions. The signal source decomposition process in WPT can provide a relatively stable transformation and inverse transformation.

Firstly, define the wavelet packet function:

$$W_{i,b}^{c}(t) = 2^{\frac{j}{2}}W^{c}(2^{j}t - b)$$

Where j represents the level of tree and b ($b = 0, 1, ..., 2^{j}$ -1) is the node index in level j. c=0, 1, ...2 j is the oscillation parameters. The process of decomposition is subject to the following recursive relation:

$$W^{2c}(t) = \sqrt{2} \sum_{b} \omega(b) W_{1,b}^{c}(2t - b)$$

$$W^{2c+1}(t) = \sqrt{2} \sum_{b} \theta(b) W_{1,b}^{c}(2t-b)$$

Where ω $(b)=\frac{1}{\sqrt{2}}\langle \varphi(t), \varphi(2t-b)\rangle$ and $\theta(b)=\frac{1}{\sqrt{2}}\langle \psi(t), \psi(2t-b)\rangle$ are the filter coefficients of low-pass and high-pass filters respectively. $\varphi(t)$ and $\psi(t)$ are scaling function and mother wavelet function respectively. $\langle \cdot, \cdot \rangle$ is the inner product operator, which was used to calculate the wavelet packet coefficients $C_{j,b}^c$ using mixture EEG signal $S_M(t)$ and wavelet packet functions $W_{i,b}^c(t)$.

$$C_{j,b}^c = \langle S_M, W_{j,b}^c(t) \rangle = \int_{-\infty}^{\infty} S_M(t) W_{j,b}^c(t) dt$$

The EEG data were decomposed using WPT into a series of frequency bands. The decomposition levels were determined by the order of 2^j , where j represents the decomposition level. This decomposition is depicted as a binary tree structure, comprising multiple nodes each with equal bandwidth. At each level, the signal was divided into 2^j equalwidth frequency bands. We achieved a multi-resolution representation of the EEG by sequentially reconstructing the coefficients at each node, progressing layer by layer in the tree structure. The process of separating distinct sub-signals through this method is illustrated in Fig. 3.

The selection of both the decomposition order and the wavelet basis function is crucial for the efficacy of WPT. The Daubechies wavelet was utilized in our study, particularly because of its ability to extract localized time-frequency features and effectively capture spikes and nonlinear EEG features [30]. Additional, the selection of decomposition

order requires adequate frequency resolution, while keeping the computational load reasonable. Specifically, j=4, 5, or 6 are common choices for EEG signals. Therefore, we chose the Daubechies 4 wavelet with a decomposition order of j=6.

2.3. Unsupervised cluster based on dynamics process of manifold learning

Multisensory interactions have traditionally been analyzed using peak-based analyses of ERP voltage waveforms [31]. Therefore, extracting a local geometric approximation of peaks from nonlinear mixtures presents a promising approach for achieving accurate signal separation. Previous research has demonstrated that manifold learning can approximate the geometric structure of ERP data without pre-existing knowledge, effectively capturing the dynamic features inherent in the underlying neural phenomena [32]. Additionally, manifold learning can extract locally linearized structures from nonlinear signals, providing a pathway to discern discriminative information from multi-resolution sub-signals.

Among various manifold learning strategies, Local Tangential Space Alignment (LTSA) demonstrates superior clustering performance compared to isometric feature mapping and locally linear embedding methods. Its primary aim is to discover nonlinear embedding in a low-dimensional representation of data that effectively preserves neighborhood relations on the manifold. Therefore, we performed LTSA to extract low-dimensional features embedded in nonlinear high-dimensional feature matrix. The main steps of LSTA are.

(1) Local Tangent Space Establishment:

Consider a dataset $MF = [w_1, w_2, ... w_2]$ constructed by WPT, for each element w_I within the dataset, its k-nearest neighbors were identified by calculating the Euclidean distance of similarity:

$$\mathit{MF} = \left[w_{I_1}, w_{I_2}, ... w_{I_k}\right]$$

Where w_I is the I-th sub-signal decomposed from WPT, $I_1, I_2, \ldots I_k$ denote the indices of these nearest neighbors within the dataset. Then, a tangent space was estimated based on the differences between neighboring points and the central point. Within this tangent space, the coordinates of each point could be linearly represented by computing d largest right

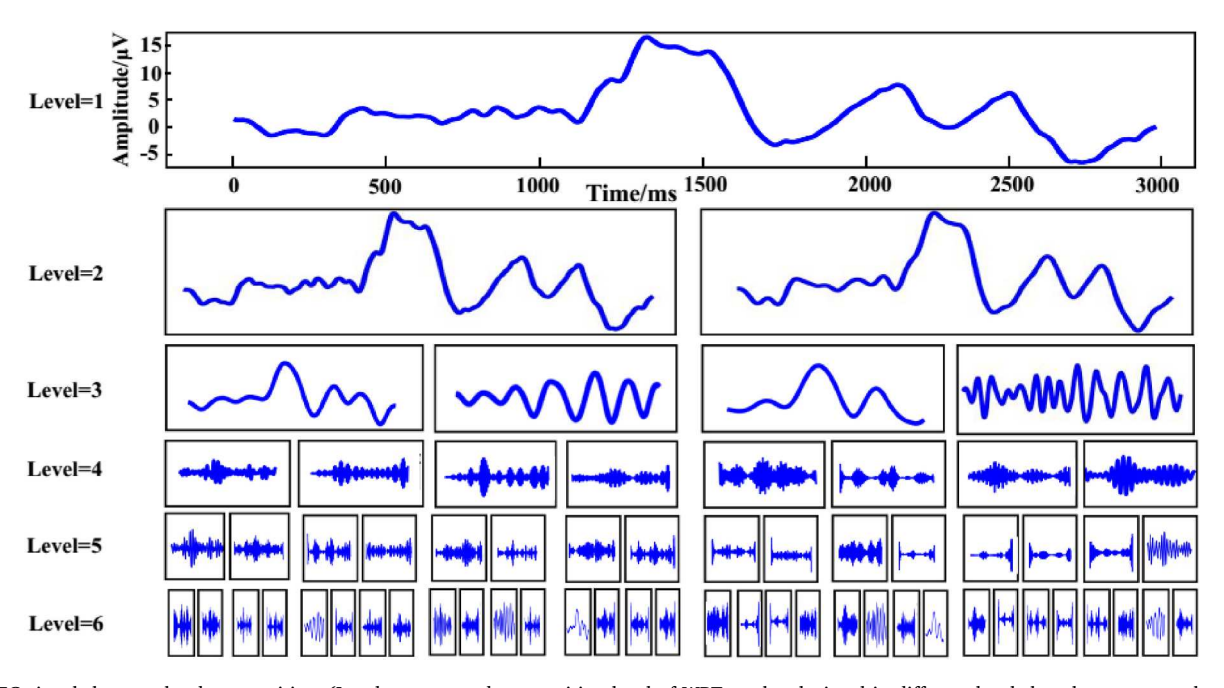


Fig. 3. EEG signals by wavelet decomposition. (Level represents decomposition level of WPT, each sub-signal in different levels has the same sample points and time duration).

singular vector of w_I .

$$V_I = [g_1, g_2, ..g_d]$$

Where V_I is vector that represents linear features, d is the intrinsic dimensionality.

(2) Alignment Matrix Construction:

This step finds a low-dimensional representation that could reconstruct all coordinate vectors across all local tangent spaces. A matrix was constructed where each block corresponds to the differences between a specific point and its neighbors, which enables the minimization of reconstruction error in the transformation from high-dimensional to low-dimensional space. To construct the alignment matrix, we firstly performed the calculation of 0–1 selection matrix:

$$H_i = (MF)^{-1} w_I$$

Where H_I is 0–1 selection matrix for w_I . Then, compute correlation matrix Z_i :

$$Z_i = I - \left[rac{e_k}{\sqrt{k}}, V_I
ight] \left[rac{e_k}{\sqrt{k}}, V_I
ight]^T$$

Where I is the identity matrix, e_k represents a column vector with all identity elements of 1. Based on the previous calculation, the alignment matrix B was constructed:

$$B = \sum_{I=1}^{I=N} H_I Z_I Z_I^T H_I^T$$

(3) Global Coordinates Alignment:

The objective of this step is to minimize the reconstruction error of matrix B by solving a series of eigenvalue problems. D-dimensional global coordinates were obtained by sorting eigenvalues and eigenvectors and extracting the first d+1 eigenvectors:

$$MFM = [u_2, u_3, ..., u_{d+1}]$$

Where MFM is d-dimensional global coordinates, u_i is eigenvectors. Eventually, we obtained the coordinates of the data points on the manifold in a low-dimensional space.

The effectiveness of LTSA can be influenced by the intrinsic dimension d and neighborhood size k. Previous research [32] reported that the first-dimensional space in the manifold features reveals the principal nonlinear waveform structure of ERP. Consequently, in our work, we set d=1 to extract the waveform features. A larger neighborhood size typically enhances the extraction of the global embedding of the manifold, and we selected k=30 for the neighborhood size based on a previous work [33]. By applying LTSA, all the decomposed sub-signals were transformed into the manifold space, resulting in manifold structures with distinct geometric characteristics.

Utilizing the outcomes of manifold dimensionality reduction allows for an approximation of the linear local structure of the signals, effectively extracting the manifold structure of various sub-signals. However, the sensitivity to parameter selection and the phenomenon of trajectory divergence of manifold structure makes it less effective in capturing dynamic processes and generating cluster features. To accurately discriminate different structure representation, we applied fuzzy entropy [34] to enhance the discriminative capability of the manifold structure. Thus, we calculated the fuzzy entropy of features extracted via manifold learning to further differentiate sub-signals based on their distinct energy and complexity index. The calculation process is described as follows:

Given a series of coordinates of manifold in a low-dimensional space $[u(1), u(2) \dots u(d)]$, the phase space dimension h ($h \le d$ -2) and the

similarity capacity limit r are defined to reconstruct the phase space. Set h as the window, which is used to divide the global coordinate series into i=d-h+1.

$$Y(i) = [u(1), u(2)...u(i+h-1) - u_0(i)]$$

$$i = 1, 2, ..., d - h + 1$$

Where Y(i) presents h consecutive u values, commencing with the ith point and generalized by removing a baseline:

$$u_0(i) = \frac{1}{h} \sum_{i=0}^{h-1} u(i+f)$$

Where f = d - h + 1, and $f \neq i$.

Then, introducing the fuzzy membership function F(x):

$$F(x) = \begin{cases} 1 & x = 0 \\ exp\left[-\ln(2) \cdot \left(\frac{x}{r}\right)^{2} \right] & x > 0 \end{cases}$$

For i = 1, 2, ..., d - h + 1, the function is:

$$F_{ij}^h = exp \left[-ln(2) \cdot \left(\frac{d_{if}^h}{r} \right)^2 \right]$$

Among them,

$$D_{if}^{h} = D[Y(i), Y(f)] = \max_{p=1,2...h} (|u(i+p-1) - |u(f+p-1) - u_0(f))$$

 D^h_{if} represents the maximum absolute distance between Y(i) and Y(f). Calculate the average value for i:

$$C_i^h(r) = \frac{1}{d-h} \sum_{f=1, f \neq i}^{d-h+1} F_{if}^h$$

Define

$$\varphi^h(r) = \frac{1}{d-h} \sum_{f=1, f \neq i}^{d-h+1} C_i^h(r)$$

Then, the FuzzyEn of time series could be calculated as:

Fuzzy
$$\mathit{En}(h,r) = \lim_{d o \infty} \bigl[\ln \varphi^h(r) - \ln \varphi^{h+1}(r) \bigr]$$

The parameter choices of FuzzyEn include the embedding dimension h, fuzzy power r and time delay τ . In previous research [34], the embedding dimension is recommended to set to h=2. The choice of fuzzy power is based on the standard deviation of the sequence to balance sensitivity and specificity. The time delay affects the boundary for determining similarity tolerance, with smaller integer values often preferred for fine-grained analysis. Thus, the parameters were set as h=2, r=1 and $\tau=1$ to accurately capture the dynamic features without high computation cost. Given that fuzzy entropy requires a vector as input and the manifold structure contains three-dimensional spatial information, we extracted the first-dimensional structure within the manifold space for subsequent fuzzy entropy calculations. This approach enabled the assessment of the dynamical processes associated with the manifold structure of each sub-signal.

2.4. Optimization of signal reconstruction based on NMF multi-channel weighting

The optimal selection of EEG channels can impact the effectiveness of feature extraction and source reconstruction [35–38]. Different combinations of specific channels can affect the detection of ERPs. Previous research has identified components that significantly contribute to specific source signals derived from multiscale sub-signals

[19]. However, the influence of different channel combinations on the reconstruction of source signals has yet to be fully explored. ERP involves processes such as trial averaging and channel averaging, which are essential for feature representation and waveform construction.

The covariance matrix of EEG data typically indicates the correlation of different brain region activities and reveals spatial patterns. These patterns are often utilized to develop models for feature extraction. Investigating these spatial superposition patterns for mixture signal could facilitate the amplitude separation of mixed ERPs, which could be achieved by determining the degree of channel contribution to different components. Because our algorithm involved only unsupervised learning, the decomposition process must rely on the intrinsic structure of the data. NMF is a computational method widely used in biomedical signal processing [39], particularly for decomposing data into components with non-negative entries. This approach serves as an unsupervised clustering method to extract components of different classes from the original data. The features extracted through fuzzy entropy were employed for clustering, resulting in the cluster of sub-signals into two different categories. Subsequently, sub-signals from each category were reconstructed to form the separated signal X, which retain the same channels and sample data points with raw EEG. Furthermore, we applied channel weighting to enhance the reconstruction of the source signal based on NMF, drawing on methodologies from previous research [40]. The pseudocode of the calculation is depicted in Fig. 4.

The NMF decomposition involves selecting a separation factor v. The channel optimization essentially entails multiplying different channels by distinct weights. Different weights can lead to varying reconstruction outcomes. We selected 14 different separation factors, ranging from 3 to 17, to calculate the weights of each channel after decomposition. Using a set of separation weights with the largest variance for channel optimization could result in more effective decomposition, which was adopted in our study.

Subsequently, we applied a hybrid channel optimization strategy to two signals separated from the mixture. Specifically, for the separated signal demonstrating higher correlation with the mixed signal, reconstruction involved combining the target components (separated signal

multiplied by the separation weight) of the current signal with the nontarget components (separated signal multiplied by the complement of the separation weight) of another separated signal. For the separated signal with lower correlation with the mixed signal, its target components were directly utilized to represent the reconstructed source. Details of the NMF optimization process are illustrated in Fig. 5.

2.5. Evaluation strategy for the developed method

To evaluate the performance of our approach, similarity of waveform, distance of latency and relative difference of amplitude (DA) were calculated to compare the similarity between the true source signal and our reconstructed source signal. Specifically, DA was employed to determine if the separation algorithm displays a preference for signals within certain temporal intervals. We selected time points ranging from 100 ms to 400 ms, averaging every 50 time points to calculate the relative difference in amplitude (DA). This calculation was conducted to ascertain the separation accuracy, as outlined in the following equation:

$$DA = \frac{Compared\ Signal - Source\ signal}{Source\ signal}$$

Moreover, we compared the separation accuracy of different approaches to validate the superiority of our algorithm in separating mixture signal and verify the efficacy of NMF in enhancing amplitude reconstruction accuracy. The separation accuracy was defined as:

$$Separation\ Accuracy = \frac{1}{DA}$$

For comparison, we also used fast independent component analysis (FastICA) [41], FastICA combined with NMF, and manifold clustering without NMF (MC) as benchmark methods. Specifically, FastICA is a common blind source separation algorithm, capitalizing the non-Gaussianity of the signals. The algorithm commences with the preprocessing of observed data, involving centering and whitening, followed by an iterative process that accentuates non-Gaussianity, predominantly quantified via negentropy, through a fixed-point iteration

Algorithm: Non-Negative Matrix Factorization for channel optimization of ERP

Input: $X^{t \times m}$, X represent separation signal after manifold cluster

Output: X_w

Condition: $q \ll \min[m, t]$

1. Calculate the variance matrix of EEG

$$X_v = \frac{X \cdot X^T}{trace(X \cdot X^T)}$$

2. Define the cost function

$$F_c(E,P) = \frac{1}{2} \left\| X_v - P \times E \right\|$$

3. Factorization

$$X_{v} = P^{n \times q} E^{q \times n}$$

4. Update rule

$$E_{\Lambda}^J \leftarrow E_{\Lambda}^{J\circ} \frac{X_v P_J}{R_{\Lambda}^n P_J + \varepsilon}$$

 ε is sparsity parameter

$$P_J \leftarrow P_J^{\circ} \frac{\sum_{\Lambda} E_{\Lambda}^J [X_{\nu} + (R_{\Lambda}^n P_J) P_J]}{\sum_{\Lambda} E_{\Lambda}^J [R_{\Lambda} + (R_{\Lambda}^n P_J) P_J]}$$

5. Normalize P_I

$$P_J = \frac{P_J - \min(P_J)}{\max(P_J) - \min(P_J)}$$

6. Calculate root mean square deviation (RMSD) between P_J and reference P_q (P_q is the straight line of 0.5 amplitude)

$$Rs = RMSD(P_I, P_a)$$

7. Channel Optimization for EEG

$$X_w = max(Rs)$$

Fig. 4. Algorithm diagram of NMF for Channel Optimization. (**Annotation**: X_{V} is covariance matrix of EEG; F_{c} is the Euclidean cost function; P is the basis matrix; E is the activation matrix and P, $E \ge 0$; Q is the rank of matrices P and E; Q is the element wise multiplication; sparsity parameter is Q; Q is the calculated weights).

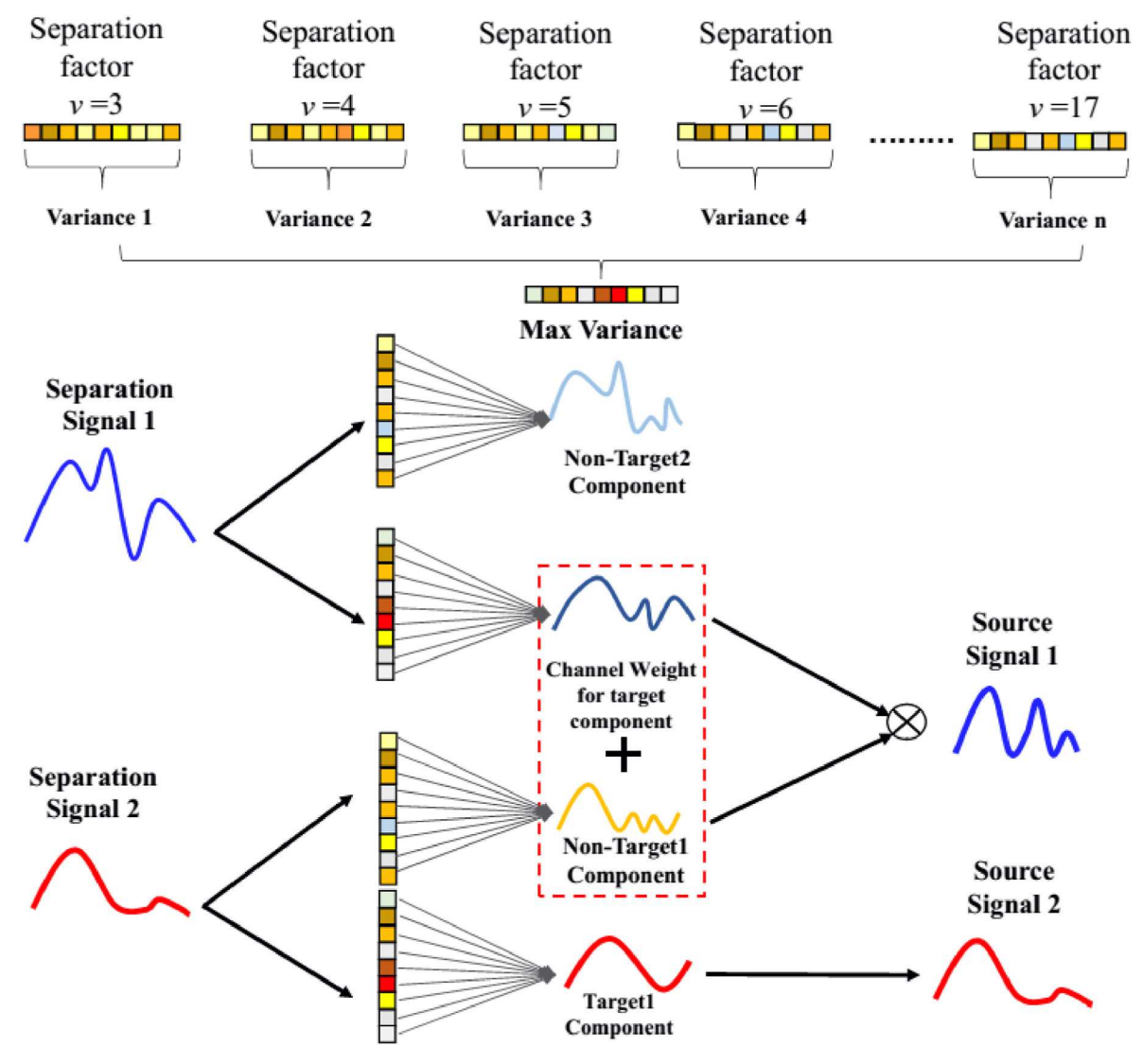


Fig. 5. Diagram of NMF multi-channel weighting. The square grids in the first row are EEG channels and different colors represent different weights. In the second row, the separation signal is reconstructed by sub-signals from each cluster. Target component is calculated after channel optimization, i.e., separation results multiply channel weights. Non-target component is the separation results multiply complement of channel weights (1-channel weights). Source signal is the reconstructed source signals after our separation method.

scheme. This approach effectively separates mixed signals into individual components by exploiting their statistical independence and the non-Gaussian nature of data. The calculation is as follows:

First, perform mean removal and whitening for mixture signal. Then, iteratively find the demixing matrix *A*:

$$a = A[:, \partial]$$

$$A_{\partial}^{\gamma+1} = \frac{1}{t} \sum_{t=1}^t S_M \tanh \left(A_{\partial}^{\gamma} \cdot S_M(t) \right) - A_{\partial} \left(\frac{1}{t} \sum_{t=1}^t 1 - \tanh^2 \left(A_{\partial}^{\gamma} \cdot S_M(t) \right) \right)$$

Where $A_{\partial}^{\gamma+1}$ and A_{∂}^{γ} are new and old separation vectors; $S_M(t)$ is observation vector at a particular point. The iteration process is terminated when the absolute value of the difference between the old and new weight vectors falls below a predefined convergence threshold.

To avoid validation testing bias, five datasets were prepared as the training set, and one dataset served as the test set. Each dataset had the opportunity to serve as the test set, through a five-fold cross validation. Additionally, we conducted a repeated measures Analysis of Variance (ANOVA) to quantify the significant differences of ERP features between the separated signals and mixture signals and across different separation

algorithms.

3. Results

3.1. Visualization of the separation process

Unfolding sub-signals, derived from wavelet decomposition, in manifold space forms distinct manifold structures characterized by local linearity. The dynamic processes within these structures were quantified using fuzzy entropy, with a focus on their projection onto the X-axis (representing the first dimension in manifold space). The methodology and detailed calculations for this process are further elucidated in Fig. 6.

Fig. 6 demonstrates that, while multiscale signals may not capture discriminative information in the time domain, they exhibit distinct dynamic trajectory patterns within the manifold structure. Capitalizing on these differences, the sub-signals were categorized into two distinct groups. The reconstruction process for each group involved combining inverse wavelet transformations with sub-band merging, iteratively applied at each level of decomposition.

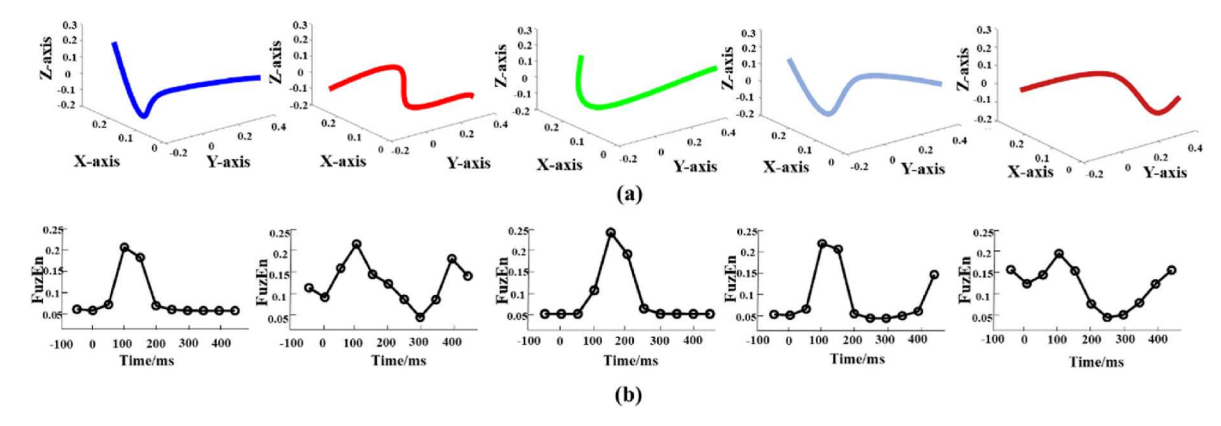


Fig. 6. Dynamic process of the manifold structure of sub-signals. (a). Manifold structure of sub-signals. (b). Dynamics process of manifold structure.

3.2. Evaluation for separation results

3.2.1. Waveform visualization for separated source signals

To evaluate the efficacy of our method in separating mixed ERP signals, we analyzed the waveform features of mixed ERP (red), real source ERP (green), and separated ERP (blue) across various simulated datasets. As Fig. 7 demonstrates, the separated signal (averaged across channels) aligns more closely with the source signal in terms of waveform features and amplitude. This alignment was particularly noticeable in the N300 components.

3.2.2. Quantification of separation results

We further compared the waveform, latency, and amplitude features of signals before and after separation against the source signal. We utilized a time window from $-100~\mathrm{ms}$ to $500~\mathrm{ms}$ relative to the stimulus input to perform a correlation analysis based on the Pearson correlation. Additionally, we computed the relative amplitude difference between the $100~\mathrm{ms}$ – $400~\mathrm{ms}$ intervals of the signal to quantify the accuracy of the source reconstruction. Detailed performance of the ERP feature comparisons averaged from two sources are presented in Table 1.

As indicated in Table 1 and Fig. 8, the separated signals exhibit a

closer resemblance to the source signal in terms of waveform, latency, and amplitude compared with the mixture signals. The repeated measures Analysis of Variance (ANOVA) revealed that the relative amplitude difference between the mixture signals and the source signal was significantly smaller than that between the mixture signals and the source signal (p < 0.01). The effectiveness of the separation process also led to an enhancement in waveform correlation (p < 0.05) and a latency that more closely approximated the source signal.

Fig. 9 shows the relative difference of amplitude at different time segments of the ERP waveform. The results showed that, across various temporal windows, the mixture signals closely replicated the source signal in amplitude. Time windows corresponding to indices 5, 6, and 7, aligning with the 200 ms–350 ms post-stimulus (the N300 component), showed the highest accuracy in amplitude reconstruction. This suggested that the algorithm was sensitive to ERP peaks during feature extraction and amplitude reconstruction. However, in some datasets, the amplitude difference in mixture signals appears smaller than in separated signal. This discrepancy may be due to situations where signals highly overlapped and the denominator was close zero, obscuring the true differences between mixture signals and separated signal amplitudes and potentially leading to inaccurate results.

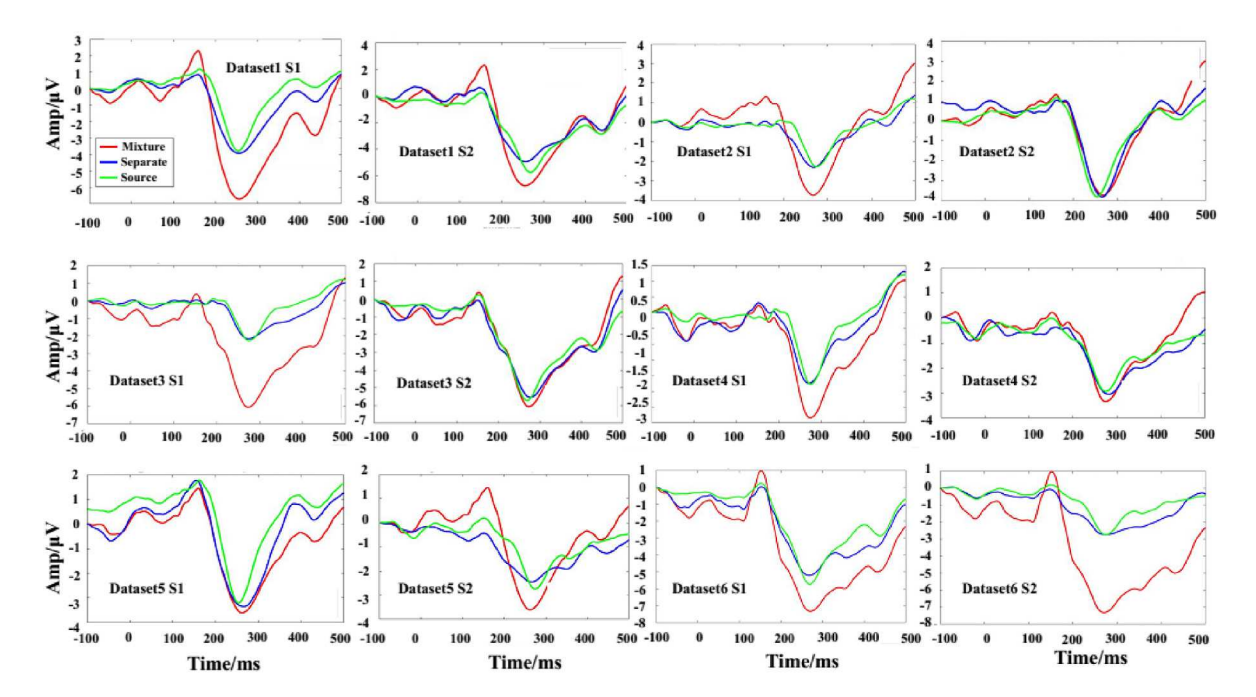


Fig. 7. Waveform of mixture ERP separated ERP and source ERP. Different panels represent different source signals of different simulated datasets. For the same dataset, the mix signal was identical for both source 1 (S1) and source 2 (S2) panels.

Table 1Quantification of ERP feature difference between separation and source signals.

	Amplitude Difference	Latency Difference	Waveform Correlation	Amplitude Difference	Latency Difference	Waveform Correlation
	Real vs Sep	Real vs Sep	Real vs Sep	Real vs Mix	Real vs Mix	Real vs Mix
Dataset 1	0.15	2.00	0.93	0.77	5.50	0.88
Dataset 2	0.25	1.00	0.92	1.08	0.00	0.87
Dataset 3	0.14	5.50	0.91	2.15	6.50	0.79
Dataset 4	0.40	1.50	0.91	0.65	2.50	0.90
Dataset 5	0.33	4.00	0.90	0.44	7.50	0.90
Dataset 6	0.37	1.00	0.91	0.67	1.00	0.89
Average	0.27	2.50	0.91	0.96	3.83	0.87

^{*}Real represents the source signal; Sep is the separated signal from mixture; Mix is the mixture signal.

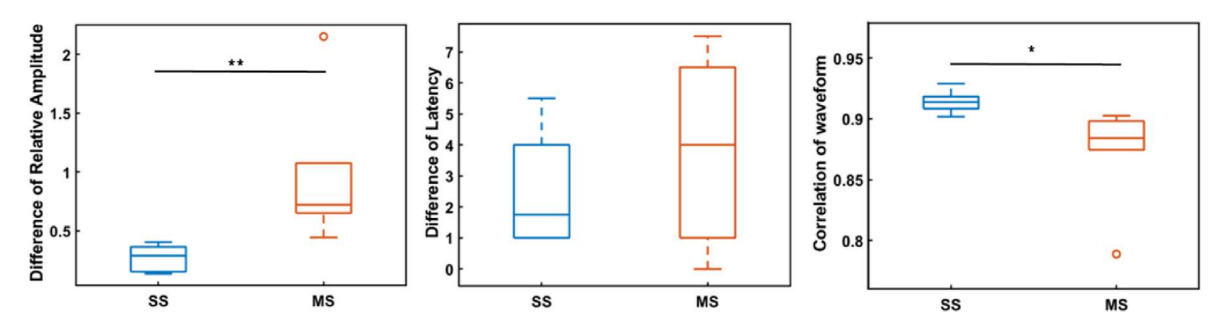


Fig. 8. Separation accuracy results (SS: Separation Signal VS source signal; MS: Mixture Signal VS source signal).

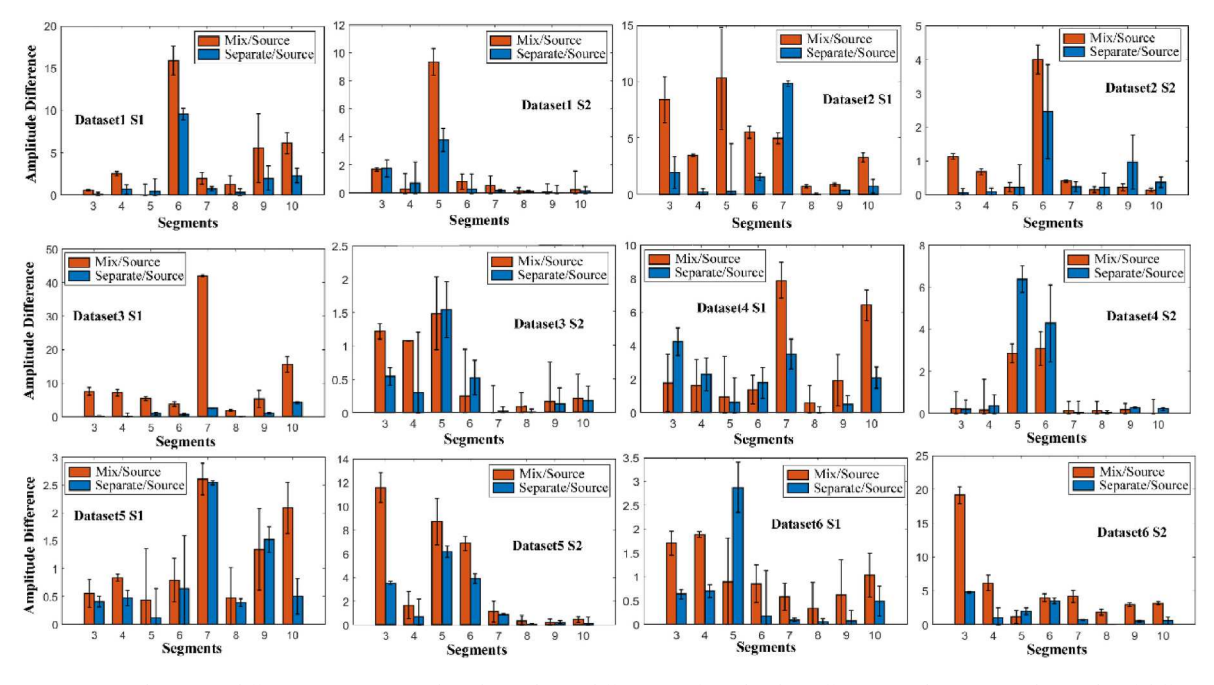


Fig. 9. Reconstruction evaluation at different time segments based on relative differences of amplitude. Different panels represent the results of different simulated datasets and source signals.

3.3. Results of comparative ablation study

We conducted an ablation study that compared the performance of different computational steps. We also compared with an existing method (FastICA). We calculated the correlation coefficient (*R*) to quantify the waveform similarity between the separated signal and the source signal (Fig. 10).

As depicted in Fig. 10 (a), manifold clustering (MC) exhibited a significant improvement after channel optimization via NMF (p < 0.001) and showed a higher accuracy than FastICA and FastICA with NMF (p < 0.001). The results showed that the reconstructed signals based on our

method achieved the highest accuracy in amplitude reconstruction. Fig. 10 (b) demonstrated that MC could effectively reconstruct the waveform features of the source signal with a higher correlation coefficient compared to FastICA (p < 0.001). Furthermore, NMF contributed to a more accurate waveform representation, achieving a correlation coefficient up to 0.9286. Without employing manifold learning and fuzzy entropy for feature extraction of sub-signals, it was difficult to obtain satisfactory performance of separation accuracy. The results demonstrated the necessity and advantages of combining the processing steps for improved outcomes. It should be noted that the amplitude reconstruction performance of signals using MC alone was found to be

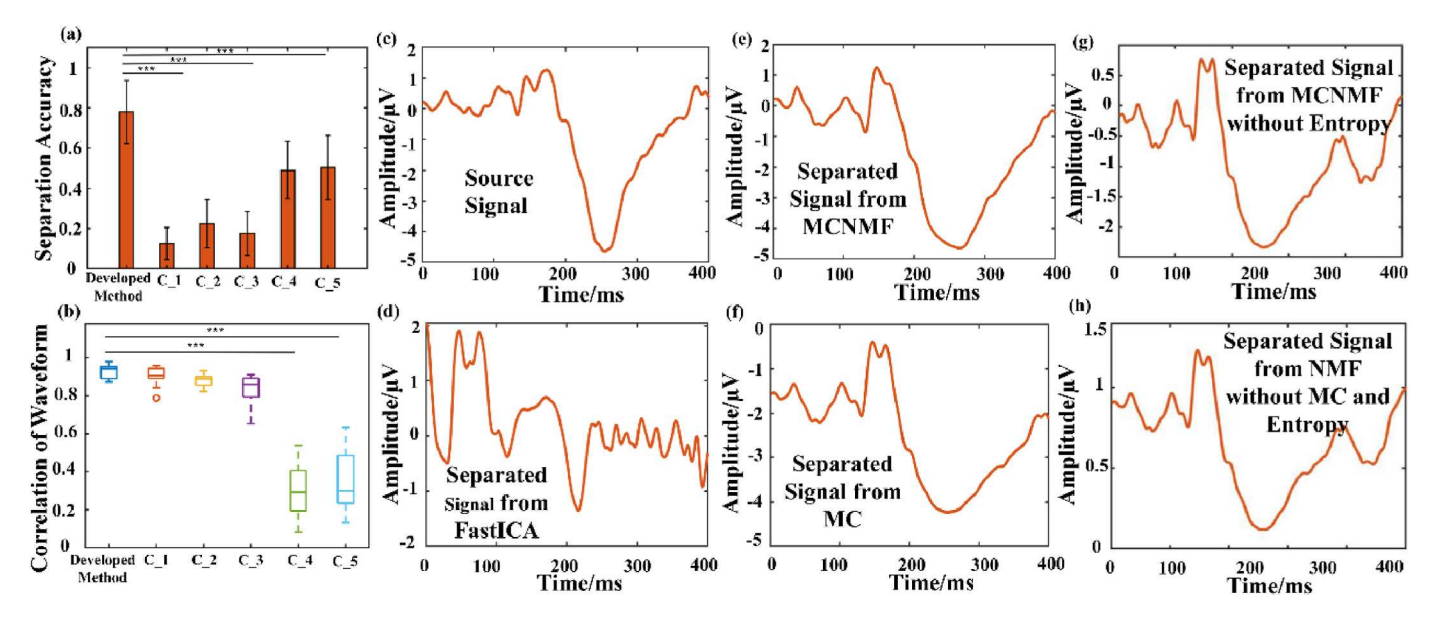


Fig. 10. (A) Separation accuracy from different strategies (C_1: Manifold Clustering (MC); C_2: Manifold Clustering and NMF (MCNMF) without entropy; C_3: NMF without entropy and MC; C_4: FastICA; C_5: FastICA with NMF). (b) Waveform correlation coefficient between the separated signal and the mixture signal. (c) An example of the source ERP waveform. (d) Separated ERP waveform calculated by FastICA. (e) Separated ERP waveform calculated by MCNMF. (f) Separated ERP waveform calculated by MCNMF without Entropy. (h) Separated ERP waveform calculated by NMF without MC and Entropy.

inferior to the decomposition results of FastICA. However, Fig. 10(c) and (d) showed that the separation waveform of FastICA was inaccurate even though the amplitude was closer to the source signal. As illustrated in Fig. 10 (f), (g) and (h), the reconstructed waveform was similar to the source signal, even though the accuracy of amplitude reconstruction was not satisfactory.

4. Discussion

This study sought to separate the individual brain responses from mixture EEG with interactive sources mixed nonlinearly. In contrast to the ICA, which separates mixed signals into additive subcomponents, our newly developed method decomposed mixed signals into source signals across different temporal and frequency scales. Subsequently, we employed source reconstruction through unsupervised clustering of subsignals based on their intrinsic nonlinear features. Additionally, NMF was implemented to optimize each channel's contribution to the source components during reconstruction, thereby ensuring a closer resemblance of the separation results to the actual source signals. Our algorithm was validated using mixed EEG signals obtained experimentally. Our results demonstrated that the mixture ERP signals were more closely aligned with the real source signals, In comparison with existing source separation algorithms.

4.1. Comparison of separation methods

In the field of neural signal identification for sensory stimulation, previous research has rarely focused on the distinct neural responses and interactions among different tactile receptors during simultaneous activation [6,42,43]. These studies often neglect the neural responses induced by non-target activations, blending the effects of co-activation with those of target activations. For instance, in tasks aimed at evaluating neural responses from finger tactile stimulation, the responses typically represent an integrated outcome of both finger and local skin tactile sensations at the site of stimulus. In EEG analysis, particularly in source interactive separation tasks, numerous research studies have advocated for various strategies employing spatial filters [44]. These filters aim to separate mixed-source stimuli by spatial projection and

linear transformation, extracting discriminative information for effective source separation. Nevertheless, the success of spatial filtering is greatly dependent on the depth of neurophysiological understanding. This includes, for example, generating template signals to decode steady-state visual evoked potentials using canonical correlation analysis [45] or understanding event-related synchronization and desynchronization dynamics for motor intention extraction from EEG using common spatial patterns [46]. Unsupervised Deep learning methods indeed have demonstrated promising performance in classifying nonlinear signals. However, our research objective was to isolate the source ERPs for individual stimuli from mixture ERP without any prior knowledge or label. The method developed in this study, along with the comparative method (FastICA), are analytical approaches that do not require any knowledge to extract the source components from mixture signals. In contrast, deep learning models learn the underlying structure, patterns, and features of signal through a large dataset. The output of this type of black-box models typically cannot be used to directly capture the source component signal. Additionally, without any target orientation or loss function, deep learning models also face challenges during implementation for source separation. Our current work developed an alternative approach focusing on isolating individual neural responses through source signal reconstruction, rather than spatial filtering, which presents a new paradigm in EEG source separation.

In this study, we employed a function characterized by nonlinear and interactive mixing strategy to simulate our EEG dataset. This function was selected for its effectiveness in preserving source mixing relations and generating highly realistic ERPs, notably featuring a typical N/P component and reasonable latency. A key concept in our work is the extraction of intrinsic features of sub-signals across time-frequency scales, a process that does not inherently necessitate the solving of nonlinear equations. Therefore, simulation with multiple nonlinear functions may not substantially contribute to the results of our algorithm validation.

Traditional blind source separation methods are proficient in handling linear stationary processes, but they are often inadequate for capturing the complexities of biological systems like the human brain, which tend to function as nonlinear dynamical systems [6]. These methods typically fail to account for the complex nonlinear behaviors

exhibited in EEG signals. Linear and stationary analyses usually overlook the variations in manifold morphology that are characteristic of nonlinear EEG time series. This oversight presents a significant challenge in developing effective discriminative boundaries for clustering. In our research, we have addressed this limitation by unraveling sub-signals of various scales into manifold structures through manifold learning. Subsequently, these structures were transformed into dynamic trajectories using fuzzy entropy. By examining the dynamic properties of these trajectories, we could extract discriminative information accurately. This methodology provides a new perspective in analyzing the dynamics of EEG signals and contributes to the development of more sophisticated clustering or classification models for complex neural signals of different modalities.

The amplitude reconstruction results indicate that the source signal reconstruction accuracy is the highest near the characteristic N/P wave peak of ERP signals. This high accuracy is likely attributed to the deterministic nature of the evoked responses in ERP signals. Notably, the waveform of the characteristic N/P wave peak remains consistent across various sub-signals, as opposed to the more variable waveforms observed at other intervals. As a result, the manifold structure features predominantly represent the nonlinear characteristics near the peak values. This finding also explains the trend observed in the fuzzy entropy profiles, which mirrors the waveform representation of the N/P peaks.

4.2. Necessity for the separation steps

It is important to note that independently observing responses from targeted electrical stimulation in sensory stimulation tasks pose significant challenges from an experimental standpoint. Specifically, it is difficult to activate tactile sensation in the fingers independently without stimulating the local skin receptors. Therefore, the task of separating individual neural responses essentially represents an unsupervised learning process, devoid of any label information. Consequently, while current deep learning models are advantageous in feature extraction for nonlinear signals, they also face challenges in separating individual responses, particularly when dealing with limited and unlabeled datasets. This limitation highlights the complexity involved in accurately isolating neural responses in the context of sensory stimulation tasks that activate multiple neural sources (sensory nerves and skin receptors).

Even though brain signals derived from scalp electrode arrays have limited spatial resolution and the signals measured from the scalp reflect the superposed activities of various neural generators, which cannot be fully delineated as mechanisms of individual neural sources. This question pertains to whether the observed neural activity represents the cumulative effect of multisensory integration in sensory coding and decision formation [47,48]. Our findings show that, compared with the mixture ERP signals, the separated ERP source signals offer a closer approximation to the actual response patterns. Our developed algorithm provides a novel tool for understanding the neural effects of individual sensory perception.

4.3. Selection of evaluation methods

Our objective was to reconstruct the ERP waveforms for individual stimuli. The most significant features of the ERP include the ERP amplitude (wave peak), latency, and waveform profiles. Therefore, three evaluation metrics (difference of amplitude, difference of latency, and similarity of waveform based on correlation) were used in this study. These metrics are the intuitive ways to evaluate the separation performance. In addition, the relative difference of amplitude directly quantified separation errors in amplitude differences after averaging time domain sample points, thereby segmenting the ERP signals into different time segments to highlight the waveform reconstruction accuracy of ERP components. Consequently, the assessment metrics utilized in this study are intuitive and comprehensive. Previous studies

have applied similar evaluation metrics to assess the performance of neural decoders. For example, earlier studies have utilized waveform correlation to measure the relation between decoder predicted motor output and the ground truth. This evaluation facilitated the optimization of decoders, enabling the continuous prediction of motor output in real-time with high levels of robustness [49]. Paul et al. implemented adaptive segmentation of EEG and then compared amplitude differences across different sub-segments for the classification of distinct sleep modes [50]. Thus, these methods have been demonstrated to be reliable in the processing of neural signals.

4.4. Limitations

One limitation of our study is that the reconstruction method for source signals relies on sub-signals from various observational scales, which rely on the performance of the decomposition algorithm. Because the decomposition process does not undergo transformation or separation at the feature level, the reconstructed source components may not fully capture the real source components. Therefore, improving and optimizing the decomposition strategy for more accurate source reconstruction is necessary in future studies. Another limitation involves the algorithm's dependency on parameter settings. The effectiveness of manifold learning, fuzzy entropy, and NMF is directly related to the choice of parameters. Consequently, the selection and optimization of these parameters entail a certain computational cost in practical applications. Furthermore, given the significant variability in EEG representation across different subjects and tasks, there is a need to explore strategies that reduce parameter dependency and enhance robustness and performance in various separation tasks. Another limitation lies in the EEG signals, which contain collective activities of brain response. The brain responses to external events will likely be multi-modal in addition to the experimental stimuli, and the brain responses are also sensitive to cognitive state of the subjects. Previous work has suggested that a crucial aspect of isolating brain responses induced by external inputs involves distinguishing the neural dynamics inherent to specific brain regions from those dynamics merely resulting from external stimuli [46]. Therefore, our developed approach does not account for the potential influence of the intrinsic dynamic characteristics on the separation process. A potential improvement could involve using EEG signals during rest as a reference to extract the intrinsic dynamic features, thereby further refining the separation algorithm.

5. Conclusion

In summary, our study developed an algorithm to separate individual components of EEG from mixture models with nonlinear and interactive sources. An unsupervised learning strategy combined with manifold cluster and NMF were performed to extract discriminative features from the perspective of nonlinear dynamics and eventually achieved an accurate signal separation. ERP simulated datasets and quantification analysis were executed to validate the performance and effectiveness of our method. Our results showed that source components from complex mixed models could be accurately reconstructed by clustering dynamic features of multi-resolution sub-signals with various time and frequency scales. Our method provides a promising way to extract individual components of brain responses from stimulus-induced responses tasks during multisensory perception.

CRediT authorship contribution statement

Kai Zhang: Writing – review & editing, Writing – original draft, Visualization, Validation, Software, Resources, Methodology, Investigation, Formal analysis, Data curation. **Xiaogang Hu:** Writing – review & editing, Project administration, Investigation.

Declaration of competing interest

The authors declare that the research was conducted in the absence of any commercial or financial relationships that could be construed as a potential conflict of interest.

Appendix A. Supplementary data

Supplementary data to this article can be found online at https://doi.org/10.1016/j.compbiomed.2024.108700.

References

- [1] Handbook of Perception and Human Performance, Wiley, New York, 1986.
- [2] D.L. Harrington, L.A. Boyd, A.R. Mayer, et al., Formulating representations of time: an event-related fMRI study[C], in: Proceedings of the 9th International Conference on Neural Information Processing, 2002 1, ICONIP'02. IEEE, 2002, pp. 423–427.
- [3] K. Nelissen, W. Vanduffel, Grasping-related functional magnetic resonance imaging brain responses in the macaque monkey, J. Neurosci. 31 (22) (2011) 8220–8229.
- [4] S.L. Schmidt, D.T. Brocker, B.D. Swan, et al., Evoked potentials reveal neural circuits engaged by human deep brain stimulation, Brain Stimul. 13 (6) (2020) 1706–1718.
- [5] F.L. Da Silva, EEG: Origin and measurement[M]//EEG-fMRI: Physiological Basis, Technique, and Applications, Springer International Publishing, Cham, 2023, pp. 32-48
- [6] Y. Liu, W. Wang, W. Xu, et al., Quantifying the generation process of multi-level tactile sensations via ERP component investigation, Int. J. Neural Syst. 31 (12) (2021) 2150049.
- [7] M. Gondan, B. Röder, A new method for detecting interactions between the senses in event-related potentials, Brain Res. 1073 (2006) 389–397.
- [8] C. Magri, U. Schridde, Y. Murayama, et al., The amplitude and timing of the BOLD signal reflects the relationship between local field potential power at different frequencies, J. Neurosci. 32 (4) (2012) 1395–1407.
- [9] S. Di, B. Brett, D.S. Barth, Polysensory evoked potentials in rat parietotemporal cortex: combined auditory and somatosensory responses, Brain Res. 642 (1–2) (1994) 267–280.
- [10] J. Vroomen, J.J. Stekelenburg, Visual anticipatory information modulates multisensory interactions of artificial audiovisual stimuli, J. Cognit. Neurosci. 22 (7) (2010) 1583–1596.
- [11] L. Vargas, G. Whitehouse, H. Huang, et al., Evoked haptic sensation in the hand with concurrent Non-Invasive nerve simulation, IEEE Trans. Biomed. Eng. 66 (10) (2019) 2761–2767.
- [12] S.P. van den Broek, F. Reinders, M. Donderwinkel, et al., Volume conduction effects in EEG and MEG, Electroencephalogr. Clin. Neurophysiol. 106 (6) (1998) 522–534.
- [13] I. Rejer, P. Górski, MAICA: an ICA-based method for source separation in a low-channel EEG recording, J. Neural. Eng. 16 (5) (2019) 056025.
- [14] H. Hälvä, A. Hyvarinen, Hidden markov nonlinear ica: unsupervised learning from nonstationary time series, in: Conference on Uncertainty in Artificial Intelligence, PMLR, 2020, pp. 939–948.
- [15] I. Khemakhem, R. Monti, D. Kingma, et al., Ice-beem: identifiable conditional energy-based deep models based on nonlinear ica, Adv. Neural Inf. Process. Syst. 33 (2020) 12768–12778.
- [16] A. Hyvarinen, H. Morioka, Unsupervised feature extraction by time-contrastive learning and nonlinear ica, Adv. Neural Inf. Process. Syst. (2016) 29.
- [17] Y.O. Li, T. Adali, W. Wang, et al., Joint blind source separation by multiset canonical correlation analysis, IEEE Trans. Signal Process. 57 (10) (2009) 3918–3929.
- [18] S.L. Wu, C.W. Wu, N.R. Pal, et al., Common spatial pattern and linear discriminant analysis for motor imagery classification[C], in: 2013 IEEE Symposium on Computational Intelligence, Cognitive Algorithms, Mind, and Brain (CCMB), IEEE, 2013, pp. 146–151.
- [19] V.J. Samar, K.P. Swartz, M.R. Raghuveer, Multiresolution analysis of event-related potentials by wavelet decomposition, Brain Cognit. 27 (3) (1995) 398–438.
- [20] S.K. Nayak, A. Bit, A. Dey, et al., A review on the nonlinear dynamical system analysis of electrocardiogram signal, Journal of healthcare engineering (2018) 2018.
- [21] A. Deleforge, F. Forbes, R. Horaud, Acoustic space learning for sound-source separation and localization on binaural manifolds, Int. J. Neural Syst. 25 (1) (2015) 1440003.
- [22] T. Brosch, R. Tam, Alzheimer's Disease Neuroimaging Initiative, Manifold Learning of Brain MRIs by Deep learning[C]//Medical Image Computing and Computer-Assisted Intervention-MICCAI 2013: 16th International Conference, Nagoya, Japan, September 22-26, 2013, Proceedings, Part II 16, Springer, Berlin Heidelberg, 2013, pp. 633–640.

- [23] J.B. Tenenbaum, V. Silva, J.C. Langford, A global geometric framework for nonlinear dimensionality reduction, Science 290 (5500) (2000) 2319–2323.
- [24] J.S. Richman, J.R. Moorman, "Physiological time-series analysis using approximate entropy and sample entropy,", Amer. J. Physiol.-Heart Circulatory Physiol. 278 (6) (2000) H2039–H2049.
- [25] F. Schoeneman, V. Chandola, N. Napp, et al., Entropy-isomap: manifold learning for high-dimensional dynamic processes[C]. 2018 IEEE International Conference on Big Data (Big Data), IEEE, 2018, pp. 1655–1660.
- [26] T. Alotaiby, F.E.A. El-Samie, S.A. Alshebeili, et al., A review of channel selection algorithms for EEG signal processing, EURASIP J. Appl. Signal Process. 2015 (2015) 1–21.
- [27] L. Vargas, H. Huang, Y. Zhu, et al., Object shape and surface topology recognition using tactile feedback evoked through transcutaneous nerve stimulation, IEEE transactions on haptics 13 (1) (2020) 152–158.
- [28] D.A. Bridwell, S. Rachakonda, R.F. Silva, et al., Spatiospectral decomposition of multi-subject EEG: evaluating blind source separation algorithms on real and realistic simulated data, Brain Topogr. 31 (2018) 47–61.
- [29] B.A. Demirci, O. Demirci, M. Engin, Comparative analysis of ANN performance of four feature extraction methods used in the detection of epileptic seizures, Comput. Biol. Med. 166 (2023) 107491.
- [30] H. Adeli, Z. Zhou, N. Dadmehr, Analysis of EEG records in an epileptic patient using wavelet transform, J. Neurosci. Methods 123 (1) (2003) 69–87.
- [31] R.A. Stevenson, D. Ghose, J.K. Fister, et al., Identifying and quantifying multisensory integration: a tutorial review, Brain Topogr. 27 (2014) 707–730.
- [32] J. Xie, G. Xu, F. Zhang, et al., A local tangent space based approach for single-trial representation of event-related potentials[C], in: 2010 5th Cairo International Biomedical Engineering Conference, IEEE, 2010, pp. 184–187.
- [33] H. Zha, Z. Zhang, Spectral properties of the alignment matrices in manifold learning, SIAM Rev. 51 (2009) 545–566.
- [34] Z. Cao, C.T. Lin, Inherent fuzzy entropy for the improvement of EEG complexity evaluation, IEEE Trans. Fuzzy Syst. 26 (2) (2017) 1032–1035.
- [35] S.M. Pincus, A.L. Goldberger, Physiological time-series analysis: what does regularity quantify? Am. J. Physiol. 266 (4 Pt 2) (1994) 1643–1656.
- [36] J.R. Msonda, Z. He, C. Lu, Feature reconstruction based channel selection for emotion recognition using EEG[C], in: 2021 IEEE Signal Processing in Medicine and Biology Symposium (SPMB), IEEE, 2021, pp. 1–7.
- [37] A. Soler, E. Giraldo, L.M. Lundheim, et al., Relevance-based channel selection for EEG source reconstruction: an approach to identify low-density channel subsets, in: Proceedings of the 15th International Joint Conference on Biomedical Engineering Systems and Technologies (BIOSTEC 2022)-Volume 1, SciTePress, 2022.
- [38] T. Alotaiby, F.E.A. El-Samie, S.A. Alshebeili, et al., A review of channel selection algorithms for EEG signal processing, EURASIP J. Appl. Signal Process. 2015 (2015) 1–21.
- [39] N. Lu, T. Li, J. Pan, et al., Structure constrained semi-nonnegative matrix factorization for EEG-based motor imagery classification, Comput. Biol. Med. 60 (2015) 32–39.
- [40] D. Gurve, D. Delisle-Rodriguez, M. Romero-Laiseca, et al., Subject-specific EEG channel selection using non-negative matrix factorization for lower-limb motor imagery recognition, J. Neural. Eng. 17 (2) (2020) 026029.
- [41] A. Hyvärinen, E. Oja, Independent component analysis: algorithms and applications, Neural Network. 13 (2000) 411–430.
- [42] L. Vargas, J. Baratta, X. Hu, Distribution of M-Wave and H-Reflex in Hand Muscles Evoked via Transcutaneous Nerve Stimulation: a Preliminary report[C]//2021 43rd Annual International Conference of the IEEE Engineering in Medicine & Biology Society (EMBC), IEEE, 2021, pp. 5897–5900.
- [43] W. Liang, C. Qin, A. Sun, et al., Study of tactile sensation somatotopy and homology between projected fingers in residual limb and natural fingers in intact limb, IEEE Trans. Neural Syst. Rehabil. Eng. 31 (2022) 636–645.
- [44] K. Zhang, G. Xu, X. Zheng, et al., Using phase synchronization to improve the performance of spatial filter during motor imagery EEG classification[C]. Proceedings of the 2021 International Conference on Intelligent Medicine and Health, 2021, pp. 30–34.
- [45] X. Chen, Y. Wang, S. Gao, et al., Filter bank canonical correlation analysis for implementing a high-speed SSVEP-based brain-computer interface, J. Neural. Eng. 12 (4) (2015) 046008.
- [46] C. Brunner, M. Naeem, R. Leeb, et al., Spatial filtering and selection of optimized components in four class motor imagery EEG data using independent components analysis, Pattern Recogn. Lett. 28 (8) (2007) 957–964.
- [47] J.K. Bizley, G.P. Jones, S.M. Town, Where are multisensory signals combined for perceptual decision-making? Curr. Opin. Neurobiol. 40 (2016) 31–37.
- [48] P. Vahidi, O.G. Sani, M.M. Shanechi, Modeling and dissociation of intrinsic and input-driven neural population dynamics underlying behavior, Proc. Natl. Acad. Sci. USA 121 (7) (2024) e2212887121.
- [49] Y. Zheng, X. Hu, Concurrent prediction of finger forces based on source separation and classification of neuron discharge information, Int. J. Neural Syst. 31 (6) (2021) 2150010.
- [50] K. Paul, V. Krajča, Z. Roth, et al., Comparison of quantitative EEG characteristics of quiet and active sleep in newborns, Sleep Med. 4 (6) (2003) 543–552.